

JGR Space Physics

RESEARCH ARTICLE

10.1029/2021JA029752

Key Points:

- For similar solar wind forcing, increased IMF $|B_y|$ influence both substorm onset latitude and the proton isotropic boundary latitude
- Substorms are less frequent for large IMF $|B_y|$ for similar solar wind forcing
- The results indicate that the magnetotail response depends on the magnitude of the IMF B_y component

Correspondence to:






L. Holappa,
lauri.holappa@oulu.fi

Citation:

Holappa, L., Reistad, J. P., Ohma, A., Gabrielse, C., & Sur, D. (2021). The magnitude of IMF B_y influences the magnetotail response to solar wind forcing. *Journal of Geophysical Research: Space Physics*, 126, e2021JA029752. <https://doi.org/10.1029/2021JA029752>

Received 5 JUL 2021
Accepted 12 OCT 2021

The Magnitude of IMF B_y Influences the Magnetotail Response to Solar Wind Forcing

Lauri Holappa¹ , Jone Peter Reistad² , Anders Ohma² , Christine Gabrielse³ , and Dibyendu Sur^{4,5} 

¹Space Physics and Astronomy Research Unit, University of Oulu, Oulu, Finland, ²Birkeland Centre for Space Science, University of Bergen, Bergen, Norway, ³The Aerospace Corporation, El Segundo, CA, USA, ⁴CIRES, University of Colorado Boulder, Boulder, CO, USA, ⁵Narula Institute of Technology, Kolkata, India

Abstract The dynamics of substorms are known to be dominated by the North-South (B_z) component of the Interplanetary Magnetic Field (IMF), which is the most important driver of the dayside reconnection. Even though the dawn-dusk (B_y) component is also known to play a role in substorm dynamics, its effects are not yet fully understood. In this paper we study how IMF B_y modulates the onset latitude, strength and occurrence frequency of substorms as well as the isotropic boundary (IB) latitude of energetic protons. We show that the substorm onset latitude and the IB latitude are about one degree lower for large magnitude B_y ($|B_y| > 3$ nT) than for small B_y . In contrast, the substorm occurrence frequency is larger for small $|B_y|$. We suggest that the magnetotail is more stable during large $|B_y|$, requiring the magnetotail lobes (and hence the polar cap) to contain more flux to initiate a substorm compared to the situation when B_y is small.

Plain Language Summary Substorms are global magnetic disturbances in which energy stored in the Earth's magnetic field is suddenly released, leading to intense aurorae and other space weather effects. Substorms are most frequent and strongest when the magnetic field incident to the Earth at the Sun-Earth line has a strong southward component. In this paper we study how the occurrence and strength of substorms are affected by the east component of this magnetic field. We show that substorms are less frequent but stronger, with associated aurora extending to lower latitudes, when the east component is strongly positive or negative. These results help in developing more accurate space weather predictions in the future.

1. Introduction

Magnetosphere-ionosphere dynamics are determined by the solar wind and interplanetary magnetic field (IMF) forcing and the system's response to that forcing. Arguably, the most important quantity in the solar wind forcing is the rate of opening of magnetic flux, or the reconnection rate, on the dayside magnetopause. For several decades, coupling functions have been used to quantify the upstream solar wind forcing. Typically, coupling functions are proportional to the product $v^\alpha B_T^\beta \sin^\gamma(\theta/2)$, where v is solar wind speed, $B_T = \sqrt{B_z^2 + B_y^2}$ and $\theta = \arctan(B_y/B_z)$ is the IMF clock angle in the Geocentric Solar Magnetospheric (GSM) coordinate system. The exponents α , β and γ are empirically determined, for example, by maximizing correlation between the coupling function and geomagnetic indices (Lockwood, Bently et al., 2019; Newell et al., 2007; Vasyliunas et al., 1982). Because geomagnetic disturbances on the ground are also much affected by how the magnetosphere and ionosphere responds to the upstream forcing, the interpretation of these coupling functions in terms of a dayside coupling efficiency is challenging. The coupling function presented by Milan et al. (2012) is slightly different in this regard, as it was specifically designed to predict the dayside reconnection rate in units of Weber per second, or Volt:

$$\Phi_D = \Lambda v^{4/3} B_T \sin^{9/2}(\theta/2), \quad (1)$$

where $\Lambda = 3.3 \cdot 10^5 \text{ m}^{2/3} \text{ s}^{1/3}$. The coupling function coefficients α , β , γ were in this case estimated by fitting the expansion of the open magnetic flux inside the polar cap as monitored by global Far Ultraviolet imaging of the aurora during intervals when tail reconnection was assumed to be negligible.

Magnetic flux that has been opened by dayside reconnection and added to the lobes must, at some point, close again in the magnetotail (Dungey, 1961). This is most commonly achieved by magnetospheric substorms. During a substorm, open flux in the lobes are closed explosively, causing a global reconfiguration of the magnetotail from a stretched, tail-like configuration to a more dipolar configuration (Hones, 1979). On average, a substorm closes about a third of the available open flux (Milan et al., 2007). The behavior of individual substorms vary, but do in general depend on the amount of open flux available in the lobes. Specifically, it has been shown that substorms occurring at lower magnetic latitudes tend to be more intense in terms of auroral brightness (Milan et al., 2010), transpolar plasma transport (Grocott et al., 2009), and ionospheric currents (Holappa et al., 2014; Milan et al., 2019; Myllys et al., 2015; Tanskanen et al., 2002) compared to substorms occurring when the auroral oval is located at higher latitudes.

The presence of an IMF B_y component significantly alters the configuration of the magnetospheric system. The amplitude and polarity of the B_y component inside the magnetosphere are positively correlated with IMF B_y (e.g. Petrukovich, 2011; Tenfjord et al., 2015), which leads to a relative displacement of the footpoint of closed magnetic field lines between the northern and southern hemisphere (abbreviated NH and SH). This is reflected in the observed location of substorm onset, which is shifted duskward (dawnward) for positive IMF B_y and dawnward (duskward) for negative IMF B_y in the NH (SH) (e.g. Liou et al., 2001; Liou & Newell, 2010; Østgaard et al., 2011). Recent studies have also shown that auroral electrojets (Friis-Christensen et al., 2017; Holappa & Mursula, 2018; Holappa et al., 2021; Smith et al., 2017), auroral oval size (Reistad et al., 2020), energetic electron precipitation (Holappa et al., 2020) and substorm occurrence frequency (Ohma et al., 2021) respond differently to solar wind forcing, depending on the sign of IMF B_y and the dipole tilt angle (or season). For a fixed value of Φ_D , the above parameters are greater for $B_y > 0$ than for $B_y < 0$ during negative dipole tilt (NH winter and SH summer). During positive dipole tilt (NH summer and SH winter) the dependence on the B_y sign is reversed. Currently it is not understood whether these effects are due to a B_y /dipole tilt dependency in the dayside reconnection rate, or if the magnetosphere responds differently to similar levels of dayside reconnection rate.

In this paper we study how the magnitude (absolute value) of IMF B_y modulates substorm onset latitudes and occurrence rates. This is done using existing lists of identified substorm onsets from satellite-based observations based on optical (Frey et al., 2004; Liou, 2010) and particle (Borovsky & Yakymenko, 2017) signatures, as well as several independent observations based on ground magnetic signatures (McPherron & Chu, 2017; Newell & Gjerloev, 2011; Nosé et al., 2012). Furthermore, we use National Oceanic and Atmospheric Administration's Polar Operational Environmental Satellites (NOAA POES) measurements of the isotropic boundary (IB) latitude of energetic protons (Asikainen et al., 2010), which marks the equatorward boundary of proton precipitation (Newell et al., 1998; Sergeev et al., 1993). The IB latitude was found to be close to the substorm onset latitude (Meurant et al., 2007) and moves equatorward during the expansion phase (Donovan et al., 2003; Gilson et al., 2012). Thus, the IB latitude measurements provide an additional database for studying the IMF B_y -effects on substorm dynamics.

The main question targeted in this paper is: Does the magnetotail respond differently to the same levels of dayside reconnection when the IMF has a strong $|B_y|$ component compared to when it has small $|B_y|$? This paper is organized as follows. In Section 2 we present how IMF B_y modulates the onset latitude and onset frequency of substorms. In Section 3 we present the B_y -dependence of the isotropic boundary latitude. Finally, we discuss our results and give our conclusions in Section 4.

2. Effect of IMF B_y Magnitude on Substorm Dynamics

Studying the effect of IMF $|B_y|$ on substorm dynamics is challenging because the level of solar wind and IMF forcing can be very different for large and small $|B_y|$. In order to do a fair comparison we compared intervals that experienced a similar dayside reconnection rate (same value of Φ_D Milan et al., 2012) in some time interval prior to the observation.

2.1. Substorm Onset Latitude

We show statistics from two independent substorm onset lists from which the onset latitude could be determined. The identified substorms are binned according to the mean value of Φ_D during the hour before

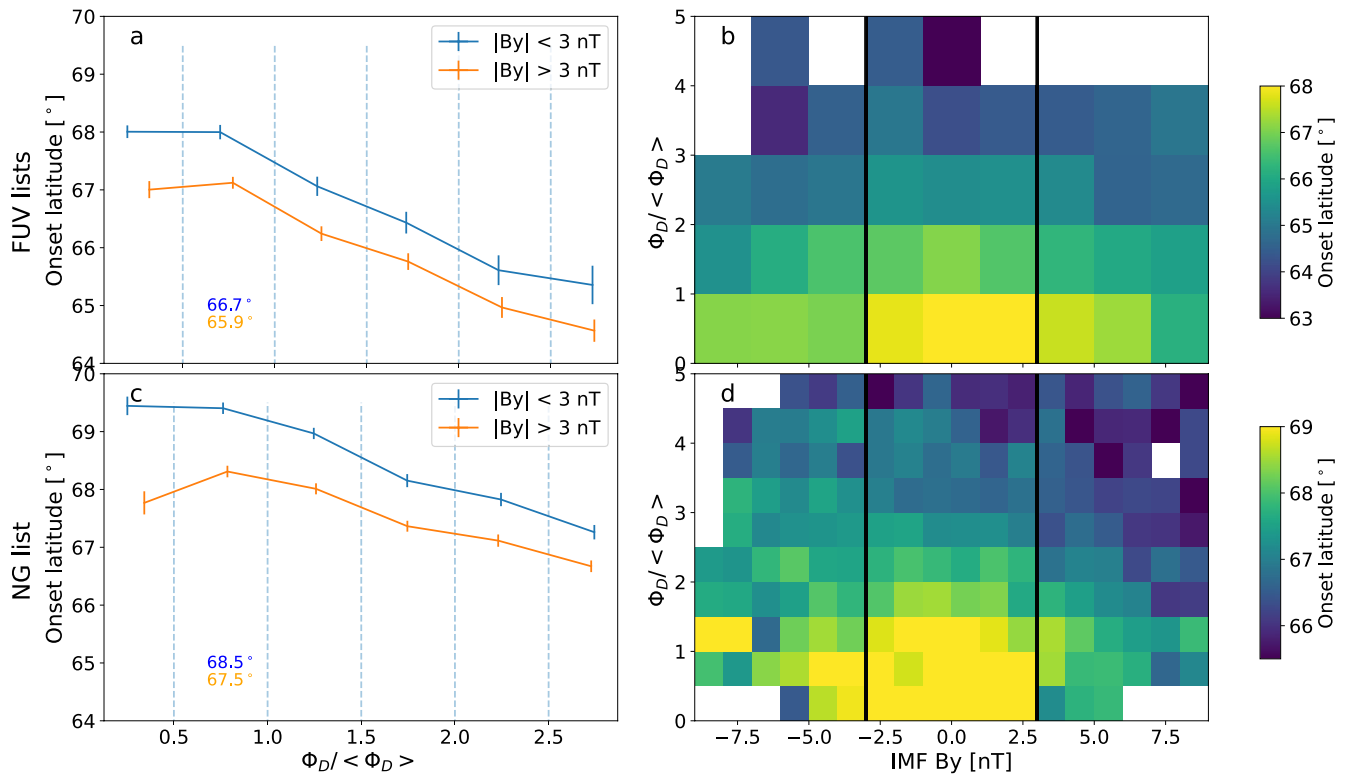


Figure 1. (a and b) Substorm onsets from the combined IMAGE and Polar FUV substorm list (Frey et al., 2004; Liou, 2010). (c and d) Substorm onsets from the NG list (Newell & Gjerloev, 2011). (b and d) 2D binning in IMF B_y (x-axis) and the $\Phi_D / \langle \Phi_D \rangle$ normalized dayside coupling parameter in the hour preceding substorm onset (y-axis). (a and c) Binning only on $\Phi_D / \langle \Phi_D \rangle$, but for large vs. small $|IMF B_y|$ separately to highlight the differences. Mean of the binned averages are printed with respective color in panels (a and c).

onset, scaled to the mean of the hourly averaged Φ_D in the period 1996 – 2019. This scaled coupling function is referred to as $\Phi_D / \langle \Phi_D \rangle$ in all figures. The hourly average values of Φ_D are based on minute resolution IMF and solar wind observations from the OMNI dataset (King & Papitashvili, 2005), representing the conditions at the bow-shock nose. Furthermore, we determined if the absolute value of the mean IMF B_y is greater or less than 3 nT, to see the effect of the presence of an IMF B_y component during otherwise similar dayside coupling. The 3 nT limit was chosen to obtain a similar number of samples in the two subsets. The absolute mean IMF B_y value was also computed based on the hour prior to substorm onset. Furthermore, we require the circular variance of the IMF clock angle during the 60 min period prior to onset to be less than 0.1 (Haaland et al., 2007; Ohma et al., 2019). We define the circular variance (σ) as a function of clock-angle θ as $\sigma = 1 - R = 1 - \sqrt{\langle \sin\theta \rangle^2 + \langle \cos\theta \rangle^2}$, where the angle brackets indicate the mean in the considered time interval. If the IMF direction (clock-angle) stays constant for the whole interval, $R = 1$ and $\sigma = 0$. The value of R decreases with increasing variability of the IMF direction. The circular variance criteria is met 58% of the time in the OMNI dataset in the period 1996–2019 and ensures that a small mean IMF B_y is not due to mixing of large positive and negative IMF B_y values.

Figure 1 shows the results of the onset latitudes determined by the combined FUV lists (Frey et al., 2004; Liou, 2010) in the top row (a and b) and the NG list (Newell & Gjerloev, 2011) in the bottom row (c and d). For the NG list onsets, we have only selected onsets located between -160° and 40° geographic longitude to avoid the longitude sector without significant latitude resolution in magnetometer coverage. Furthermore, we exclude onsets on the dayside (06–18 Magnetic Local Time [MLT]). The left panels (a and c) show the mean substorm onset latitude in bins of the normalized coupling function $\Phi_D / \langle \Phi_D \rangle$ for large and small values of IMF B_y , as orange and blue, respectively. Standard error of the mean values are indicated with vertical error bars, and the Φ_D binning is indicated with vertical dashed lines. The mean of the binned average values are also printed in respective color in panels (a and c). The right panels (b and d) show a 2D

binning of the onsets by the normalized dayside coupling parameter (y -axis) and IMF B_y (x -axis), and use color to represent the mean onset latitude within the grid spanned by the binning. Bin cells having 10 or less substorms are flagged white. The right panels (b and d) have black vertical lines at ± 3 nT IMF B_y , where we define large vs. small $|B_y|$. The substorm onset latitude is systematically lower in the FUV list than in the NG list. This probably reflects the fact that strong ground magnetic signatures (used in NG list) are seen only after some poleward expansion of the auroral bulge after the optical substorm onset (used in FUV list). However, in both lists, substorm onset moves to lower latitudes in response to increased dayside reconnection rate in the preceding hour, as expected. In addition, during intervals of the same dayside reconnection rate as parametrized by $\Phi_D/\langle\Phi_D\rangle$, the mean onset latitude is slightly higher when $|B_y|$ is < 3 nT compared to > 3 nT, a trend seen in all panels in Figure 1.

2.2. Substorm Occurrence Frequency

In order to address whether the substorm occurrence rate is affected by the magnitude of IMF B_y during otherwise similar conditions, we use five different substorm onset lists based on independent onset signatures:

1. Newell and Gjerloev (2011) (hereafter N&G): based on negative bays in the *SML* index. This 1-min resolution index is based on magnetometers at mainly auroral latitudes in the NH (Gjerloev, 2012) and quantifies the strength of the westward electrojet. The list includes 70,278 onsets in 1981–2019.
2. McPherron and Chu (2018) (M&C): based on positive bays in ground magnetic field at mid-latitudes. The positive bays are identified from the Midlatitude Positive Bay (MPB) index (Chu et al., 2015). This index quantifies the power of the field-aligned currents associated with the substorm current wedge. Using a threshold requiring the area of the positive bays to exceed 700 nT²-min, 57,557 onsets were found during 1982–2012.
3. Nosé et al. (2012): based on Pi2 pulsations, quantified by the Wp index. The list includes 14,075 onsets in 2005–2019.
4. The combined onset list based on global far-ultraviolet (FUV) images of the global aurora from IMAGE and Polar satellites gives 6,727 onsets during 1996–2007 (Frey et al., 2004; Frey & Mende, 2006; Liou, 2010). Note that these lists (hereafter F+L) do not provide continuous coverage, since the auroral onset feature must be within the field-of-view of the camera to be detected.
5. Borovsky and Yakymenko (2017): based on electron injections at geosynchronous orbit, yielding 16,025 onsets during 1989–2007. This onset list (B&Y) has a temporal resolution of 30 min.

We binned the onsets identified by each list by $\Phi_D/\langle\Phi_D\rangle$. We further grouped the data based on the average IMF B_y in the hour prior to each onset. Finally, we normalized the number of onsets by the number of days with IMF B_y and $\Phi_D/\langle\Phi_D\rangle$ within each bin, giving onsets per day. The onset occurrence rates are displayed in Figure 2, where each row corresponds to a different onset list. In Figures 2a, 2c, 2e, 2g and 2i, the onsets are separated by whether $|B_y| < 3$ nT (blue) or $|B_y| > 3$ nT (orange). The numbers in the upper left corner of each panel indicate the number of substorms that contribute to the statistics. To verify that any differences are statistically significant, we applied bootstrapping on the time series within each bin. By drawing 1,000 random samples of the same size as the time series in each bin (with replacement), we get an estimate of the standard error of the daily onset frequency by calculating the standard deviation of the onsets/day found in each sample. Figures 2b, 2d, 2f, 2h and 2j display the onsets grouped in 2-nT wide bins based on IMF B_y , in addition to the binning on solar wind forcing.

Figure 2 shows that substorms occur more frequently when the magnitude of IMF B_y is small. The line plots show that the daily onset frequency is significantly higher when IMF $|B_y| < 3$ nT and the 2D plots show higher values in the central columns compared to either side. The distribution for the N&G list in Figure 2b is shifted toward positive IMF B_y values, a trend first reported by Liou et al. (2020). While they suggested that this implied stronger coupling between the IMF and the terrestrial field during positive IMF B_y , Ohma et al. (2021) demonstrated that this trend is most likely a consequence of the N&G list being based exclusively on magnetometers in the NH, and that an opposite trend was found in the SH. This effect thus represents a local, hemispherical effect, and is not associated with a general, global difference between positive and negative IMF B_y . This conclusion is further strengthened by the 2D distributions shown in Figures 2d, 2f, and 2j, which appear to be centered around IMF $B_y = 0$.

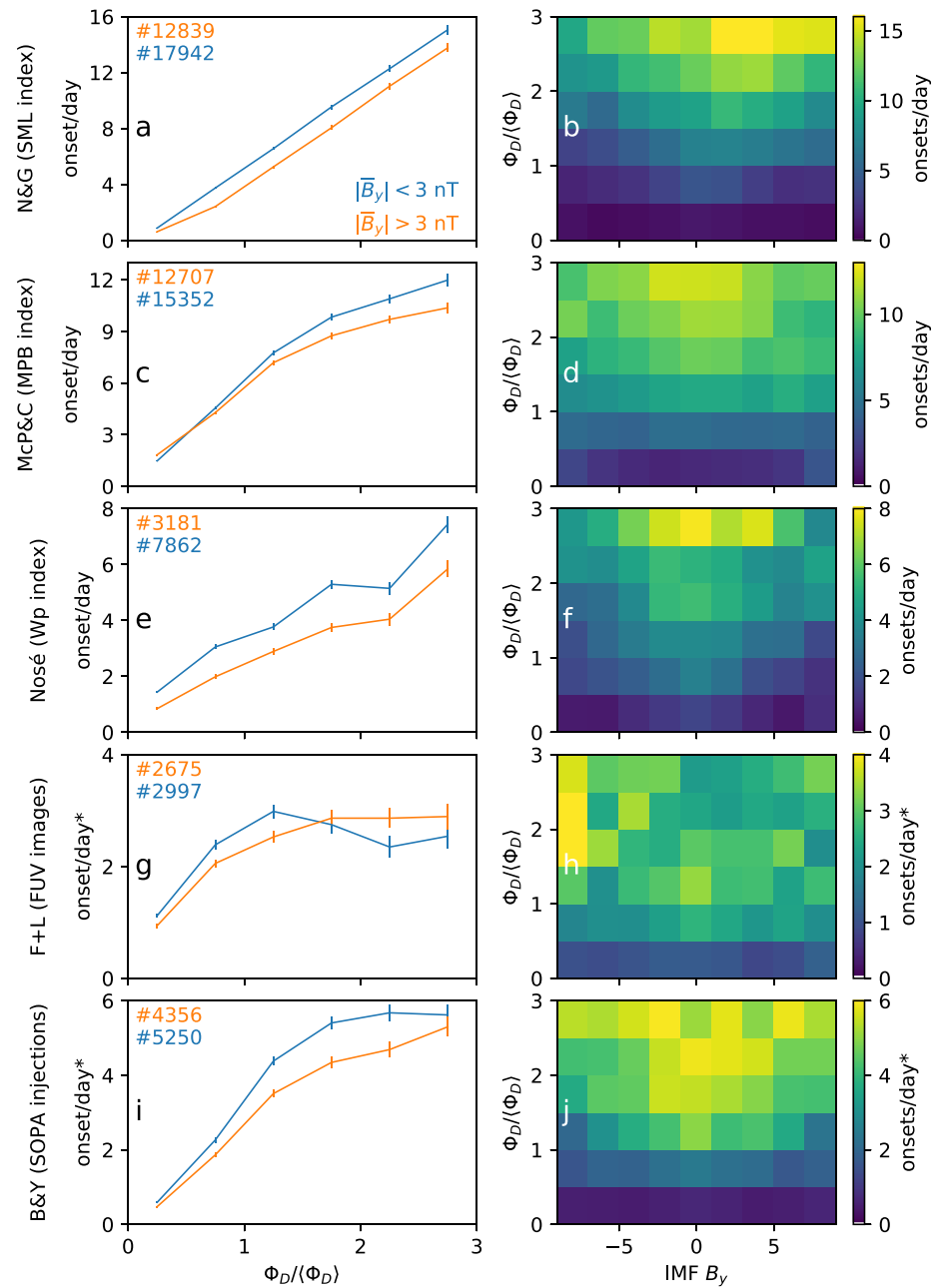


Figure 2. Daily substorm frequency. Each row corresponds to different onset lists. Left: onsets/day for small (blue) and large (orange) IMF $|B_y|$ binned by $\Phi_D / \langle \Phi_D \rangle$. Right: onsets/day binned by IMF B_y and $\Phi_D / \langle \Phi_D \rangle$. The two onset lists based on spacecraft observations have been labeled with “*” to indicate that the observed onset frequency is affected by data gaps and spacecraft location.

Consistent trends of higher onset frequency for small IMF B_y are also seen for low solar wind forcing in the F+L onset list (Figures 2g and 2h), but the results are more ambiguous for stronger solar wind forcing. However, there are several reasons to put less emphasis on these results. This list contains the fewest amount of identified onsets, which means that the statistics are poor compared to the other lists, especially in the high-forcing bins. This is reflected in the relatively larger error bars compared to the other lists. Furthermore, the normalization to the solar wind forcing is less reliable for this list, since the F+L time series is discontinuous. This is due to the fact that the IMAGE and Polar satellites cannot observe the auroral regions continuously. Therefore, the onsets/day rate cannot be calculated as reliably using the OMNI data in

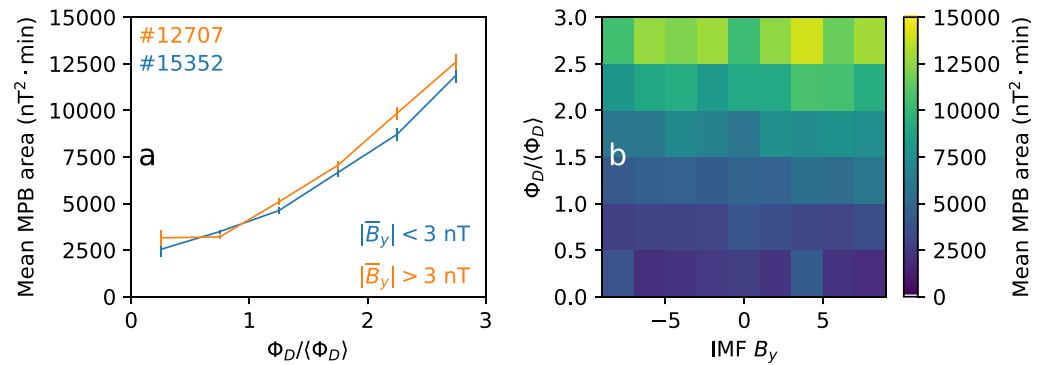


Figure 3. Mean Midlatitude Positive Bay (MPB) area based on the McP&C onset list, quantifying substorm strength. Left: mean area for small (blue) and large (orange) IMF $|B_y|$ binned by $\Phi_D / \langle \Phi_D \rangle$. Right: mean area binned by IMF B_y and $\Phi_D / \langle \Phi_D \rangle$.

the time period covered by this onset list as for the lists based on continuous, ground-based measurements. There could therefore be errors in the normalization, especially in the high-forcing bins which contain few hours of data.

2.3. Substorm Strength

We next address how the average substorm strength is affected by IMF B_y during the same levels of upstream solar wind forcing. To quantify possible differences, we used the area of the midlatitude positive bays (MPBs) identified by McPherron and Chu (2018). This quantity is proportional to the power of the substorm current wedge, and thus offers a proxy of the substorm strength. We estimated the mean value of the identified MPB areas in the same bins as used in Figure 2. The result is displayed in Figure 3. The error bars in Figure 3a indicate the standard error of the means.

Figure 3a indicates that substorms are slightly stronger for large IMF $|B_y|$ than for small $|B_y|$. This result is consistent with the observation that substorms occur at lower latitudes for large $|B_y|$ (Figure 1), as it has been shown that substorms occurring at lower magnetic latitudes are more intense in terms of auroral brightness (Milan et al., 2010) and ionospheric currents (Holappa et al., 2014; Myllys et al., 2015; Milan et al., 2019; Tanskanen et al., 2002).

3. Isotropic Boundary

In the above analysis we have shown how the magnitude of IMF B_y modulates the frequency and onset latitude of substorms. In order to quantify the magnetotail response to IMF B_y , we use the isotropic boundary latitude determined from NOAA POES measurements of energetic protons. The IB latitude marks the boundary separating the regions of full and empty proton loss cones (Sergeev & Gvozdevsky, 1995), meaning equatorward of the IB the flux of 90° pitch-angle protons becomes much greater than the 0° (precipitating) flux. The IB latitude marks the transition from dipolar to non-dipolar field-lines and is therefore located close to the equatorward boundary of the auroral oval.

The IB latitude can be determined over a wide range of MLT sectors, but it is known to exhibit a systematic MLT dependence with higher IB latitudes seen in the dusk and dawn sectors than at midnight. To take this MLT dependence into account, Sergeev and Gvozdevsky (1995) introduced the magnetotail (MT) index, which normalizes IB measurements to the midnight MLT level. The version of MT index used in this paper is described by Asikainen et al. (2010). In general, the IB latitude is a function of energy. Here we calculate the MT index for 80–250 keV protons from all available data of NOAA15–NOAA19 satellites, which have been calibrated into a single homogeneous data set (Asikainen et al., 2012).

Figure 4a shows averages of the MT index (with standard errors) for different values of $\Phi_D / \langle \Phi_D \rangle$ and IMF B_y . The MT index is calculated by averaging measurements from NH and SH. Figure 4a shows that

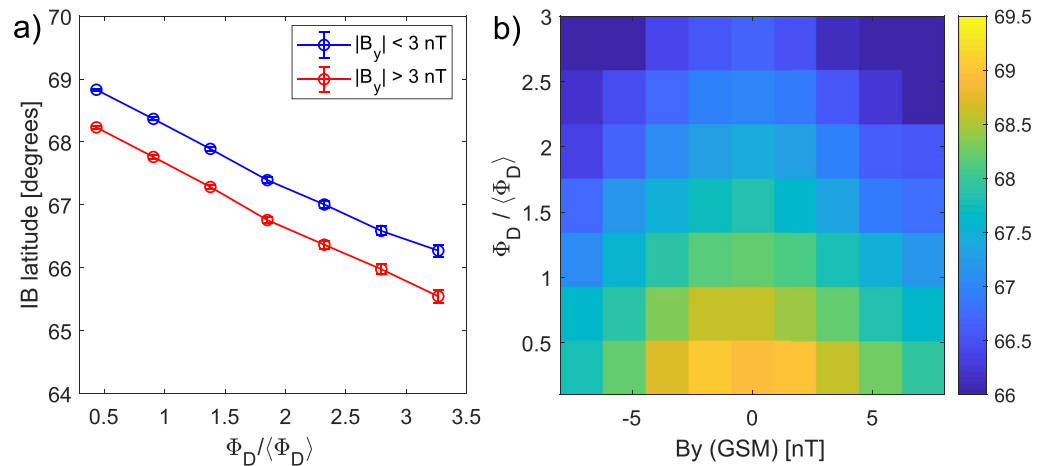


Figure 4. (a) Averages of the isotropic boundary (IB) latitude (magnetotail [MT] index) for $|B_y| > 3$ nT and for $|B_y| < 3$ nT as a function of $\Phi_D / \langle \Phi_D \rangle$. Averages are calculated from both NH and SH are averaged. (b) Averages of the IB latitude for different values of IMF B_y and the Milan coupling function Φ_D .

for a fixed value of $\Phi_D / \langle \Phi_D \rangle$, the MT index is clearly lower for large values of $|B_y|$. The B_y -dependence is symmetric with respect to the sign of B_y . Thus, the MT index shows a similar dependence on $|B_y|$ as the substorm onset latitude (see Figure 1). A comparison of Figures 1a and 4a show that for a fixed value of $\Phi_D / \langle \Phi_D \rangle$, the average substorm onset latitude is located about 1° equatorward from the IB latitude which is in excellent agreement with earlier results by Meurant et al. (2007), who found that the substorm onsets observed from IMAGE FUV images occur close to the proton IB latitude. The IB latitude is about 1 degree lower for $|B_y| > 3$ nT than for $|B_y| < 3$ nT, in agreement with the (IMAGE FUV) substorm onset latitude (Figure 1a).

4. Discussion and Conclusions

In this paper we have shown that the absolute value of IMF B_y modulates the occurrence rate and onset latitude of substorms. We showed that for a fixed value of the Milan et al. (2012) coupling function, substorms occur at lower latitudes for large absolute values of IMF B_y . In contrast, the substorm onset frequency is greater for small $|B_y|$. These results are supported by several independent substorm onset lists, based on optical satellite images, ground-based magnetic measurements, and in-situ measurements of electron injections at geostationary orbit.

In addition to substorm observations, we also analyzed the proton IB latitude. We showed that the IB latitude has a very similar dependence on IMF $|B_y|$ as the substorm onset latitude, which is in excellent agreement with Meurant et al. (2007) and Oberhagemann and Mann (2020). In our analysis we used the IB latitude averaged over both hemispheres. However, the same trends are found in each hemisphere individually, and also regardless of local season. Therefore the above dependence on $|B_y|$ is a global magnetospheric effect and not limited to only one hemisphere. Thus, these results support the above analysis based on substorm observations.

Even though a greater amount of magnetic flux is closed by strong substorms during large $|B_y|$, we have shown that they occur less frequently than weaker substorms during small $|B_y|$. Based on these results we therefore have no obvious reason to believe that the underlying mechanism is the dayside reconnection rate being significantly different for large B_y vs. small B_y . Rather, we suggest that the magnetotail is more stable during large $|B_y|$, which allows more flux to be added to the tail lobes in the substorm growth phase, resulting in larger polar cap size (and lower IB latitude) prior to the substorm onset, and less frequent onsets.

In our analysis we have used the Milan et al. (2012) coupling function Φ_D to represent the dayside reconnection rate. This empirically determined function depends on the clock-angle factor $\sin^{9/2}(\theta/2)$, and thus on IMF B_y . The exponent γ in the clock-angle factor ($\gamma = 9/2$ for Φ_D) controls the B_y -dependence of a cou-

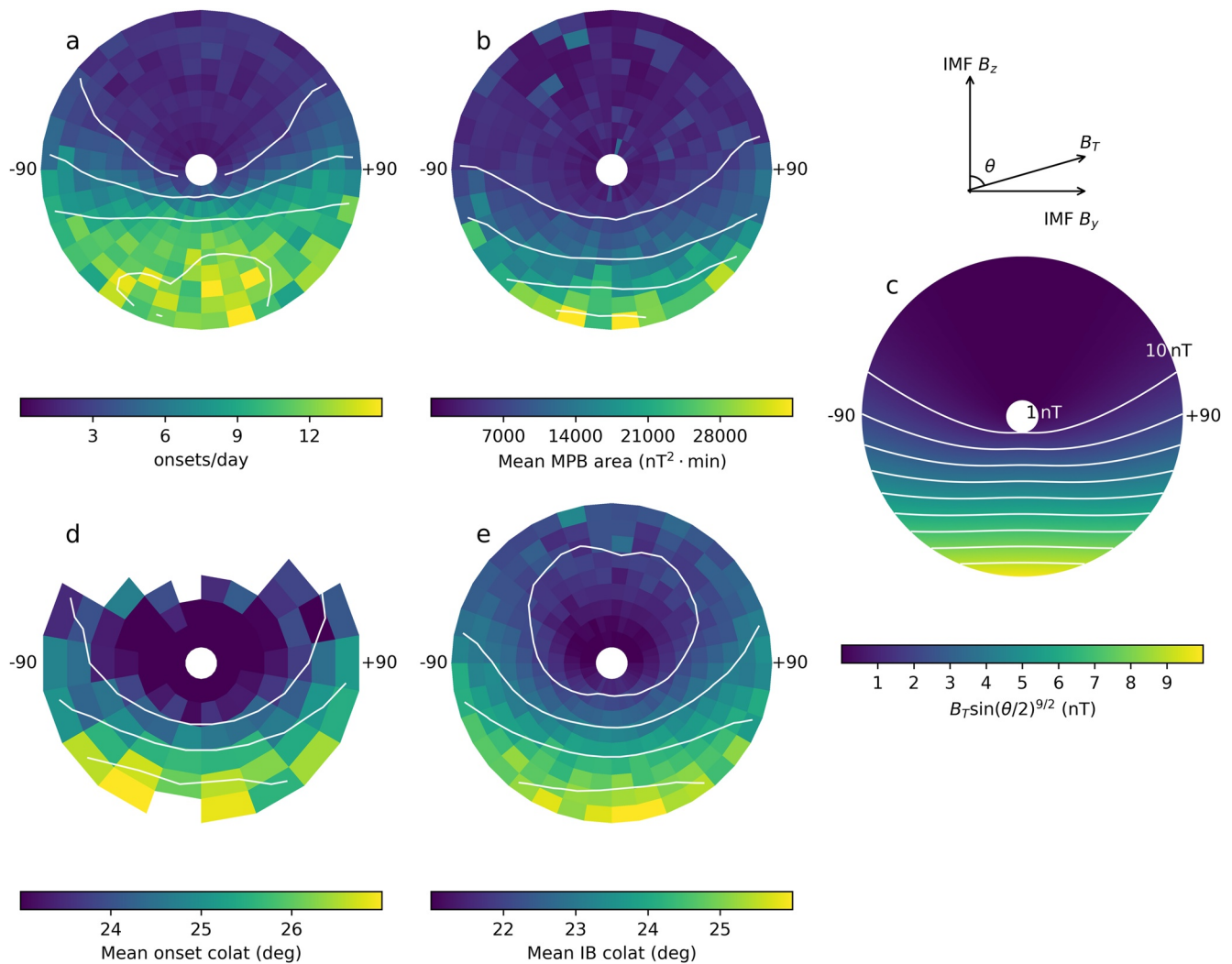


Figure 5. Averages of (a) substorm onset frequency (b) strength (Midlatitude Positive Bay [MPB] area) as a function of IMF B_T and the clock-angle θ . The substorm onset frequency and strength are based on the McP&C list. (c) Same for the Milan coupling function Φ_D . (d) Average onset colatitude based on the F+L list. (e) Average IB colatitude. Contours are marked with white lines in all panels. In all panels the radial distance from the origin denotes the magnitude of B_T (1–10 nT) while θ is measured clockwise from the B_z axis.

pling function. The exponent γ cannot be constrained theoretically, but has to be determined empirically (Vasyliunas et al., 1982). The exponent $\gamma = 9/2 = 4.5$ found by Milan et al. (2012) is close to the optimum values found earlier by MHD modeling (Laitinen et al., 2007) and by maximizing correlation with geomagnetic indices (Lockwood, 2019; Lockwood, Bentley et al., 2019). However, over the years, coupling functions with different exponents have also been proposed. Examples of well-known empirical coupling functions using significantly lower exponents than Milan et al. (2012) include Kan and Lee (1979) function (using $\gamma = 2$) and Newell et al. (2007) function ($\gamma = 8/3$).

The results of the above analysis may depend on the choice of the coupling function (mainly on the value of γ). However, our conclusions remain valid for any value of γ . To verify this, we plot averages of the substorm onset frequency and strength (based on the McPherron and Chu (2018) substorm list) for different values of B_T and clock-angle θ in Figures 5a and 5b, respectively. For a comparison, Figure 5c displays how the $B_T \sin(\theta/2)^{9/2}$ term of the Milan function Φ_D varies with B_T and θ . Comparison of Figures 5a–5c shows that contours of substorm onset frequency and substorm strength do not follow the theoretical (Milan function) contours. While the theoretical contours in Figure 5c are mostly horizontal (weak dependence on $|B_y|$) for $B_z < 0$, the contours of the substorm strength (Figure 5b) are curved, reflecting that substorm strength

increases with $|B_y|$ more steeply than Φ_D (see also Figure 3). The contours of substorm onset frequency (Figure 5a) follow the theoretical contours for weakly negative values of B_z but diverge from the theoretical contours for strongly negative B_z , when substorms are more frequent for small $|B_y|$. This reflects the trends seen in Figure 2 where most substorm lists show significant $|B_y|$ -dependence of onset frequency for strong solar wind forcing. Figures 5d and 5e show that the contours of substorm onset colatitude (from the IMAGE FUV list) and IB colatitude show a similar dependence on $|B_y|$ for $B_z < 0$ (when substorms are mainly occurring) which is consistent with Figures 1a and 4a. Also, the contours of the onset and IB colatitudes are similarly curved as the contours of the substorm strength in Figure 5b, reflecting the fact that the substorm strength increases with substorm onset colatitude. Thus, even without making any assumptions on the functional form of the optimal coupling function, we can deduce from the differences in Figures 5a, 5b, 5d, and 5e that the response of the magnetotail to solar wind forcing is indeed different during large and small $|B_y|$.

The physical mechanism of the B_y -dependence studied in this paper is not currently known. However, the underlying mechanism could be related to the B_y -component in the magnetotail. Shen et al. (2003) derived an analytic expression of the minimum radius of curvature of a closed field line passing through the neutral sheet. In their Equation D13, they show that the minimum radius of curvature of such field lines are proportional to $\sim B_y^2$ for a fixed neutral sheet thickness and B_n (B_y and B_n being the GSM y- and neutral sheet normal-component, respectively). Since B_y on closed field lines is positively correlated with IMF B_y (e.g., Cowley & Hughes, 1983; Tenfjord et al., 2015), the presence of large IMF $|B_y|$ is, as an isolated effect, expected to increase the minimum radius of curvature of the field lines in the tail. This effect may be relevant for the occurrence rate and strength/onset latitude of substorms, as thinning of the current sheet is regarded as a pre-condition for tail reconnection to take place (e.g., Schindler & Birn, 1993; Snekvik et al., 2012). It may therefore be possible that the large IMF $|B_y|$ situation on average requires more open magnetic flux to initiate a substorm due to the stabilizing effect mentioned above. That is consistent with our observations of onsets occurring less frequently and at lower latitudes when IMF $|B_y|$ is large vs. small. In a simulation study using resistive MHD, Hesse et al. (1990) found that the reconnection rate slows with increasing B_y -component in the neutral sheet. Such a mechanism could potentially explain why the magnetotail is more stable for large value IMF B_y than for small B_y . More research, including numerical modeling of the magnetotail dynamics, is needed for better understanding of the above mechanisms and whether they can explain the IMF B_y -dependencies found in this paper.

Data Availability Statement

The solar wind data were downloaded from the OMNI2 database (<http://omniweb.gsfc.nasa.gov/>). All the original POES/MEPED energetic particle data used here are archived in the NOAA/NGDC dataserer (<http://www.ngdc.noaa.gov/stp/satellite/poes/index.html>). We gratefully acknowledge the SuperMAG collaborators (<http://supermag.jhuapl.edu/info/?page=acknowledgement>). The N&G and the IMAGE FUV onset lists were downloaded from <http://supermag.jhuapl.edu>. The Wp index, from which we derived the Nosst, was downloaded from <http://www.isee.nagoya-u.ac.jp/~nose.masahito/s-cubed/>.

References

- Asikainen, T., Maliniemi, V., & Mursula, K. (2010). Modeling the contributions of ring, tail, and magnetopause currents to the corrected Dst index. *Journal of Geophysical Research*, *115*(A14), 12203. <https://doi.org/10.1029/2010JA015774>
- Asikainen, T., Mursula, K., & Maliniemi, V. (2012). Correction of detector noise and recalibration of noaa/meped energetic proton fluxes. *Journal of Geophysical Research*, *117*(A9). <https://doi.org/10.1029/2012ja017593>
- Borovsky, J. E., & Yakymenko, K. (2017). Substorm occurrence rates, substorm recurrence times, and solar wind structure. *Journal of Geophysical Research: Space Physics*, *122*(3), 2973–2998. <https://doi.org/10.1002/2016ja023625>
- Chu, X., McPherron, R. L., Hsu, T.-S., & Angelopoulos, V. (2015). Solar cycle dependence of substorm occurrence and duration: Implications for onset. *Journal of Geophysical Research: Space Physics*, *120*(4), 2808–2818. <https://doi.org/10.1002/2015JA021104>
- Cowley, S., & Hughes, W. (1983). Observation of an imf sector effect in the B_y magnetic field component at geostationary orbit. *Planetary and Space Science*, *31*(1), 73–90. [https://doi.org/10.1016/0032-0633\(83\)90032-6](https://doi.org/10.1016/0032-0633(83)90032-6)
- Donovan, E. F., Jackel, B. J., Voronkov, I., Sotirelis, T., Creutzberg, F., & Nicholson, N. A. (2003). Ground-based optical determination of the b2i boundary: A basis for an optical mt-index. *Journal of Geophysical Research*, *108*(A3). <https://doi.org/10.1029/2001ja009198>
- Dungey, J. W. (1961). Interplanetary magnetic field and the auroral zones. *Physical Review Letters*, *6*, 47–48. <https://doi.org/10.1103/physrevlett.6.47>

Acknowledgments

The work of Lauri Holappa was funded by the Academy of Finland Postdoctoral project (no. 322459). Anders Ohma was supported by the Research Council of Norway/CoE under contract 223252/F50. Jone Peter Reistad was funded by the Research Council of Norway through grant 300844/F50. This effort was facilitated by the Center for the Unified Study of Interhemispheric Asymmetries (CUSIA), NASA Award 80NSSC20K0606. Christine Gabrielse was funded by NASA Award 80NSSC20K0606.

- Frey, H. U., & Mende, S. B. (2006). Substorm onsets as observed by IMAGE-FUV. In *Proceedings of the 8th international conference on substorms* (pp. 71–76).
- Frey, H. U., Mende, S. B., Angelopoulos, V., & Donovan, E. F. (2004). Substorm onset observations by IMAGE-FUV. *Journal of Geophysical Research*, *109*(A18), 10304. <https://doi.org/10.1029/2004JA010607>
- Friis-Christensen, E., Finlay, C. C., Hesse, M., & Laundal, K. M. (2017). Magnetic field perturbations from currents in the dark polar regions during quiet geomagnetic conditions. *Space Science Reviews*, *206*(1–4), 281–297. <https://doi.org/10.1007/s11214-017-0332-1>
- Gilson, M. L., Raeder, J., Donovan, E., Ge, Y. S., & Kepko, L. (2012). Global simulation of proton precipitation due to field line curvature during substorms. *Journal of Geophysical Research*, *117*(A5). <https://doi.org/10.1029/2012ja017562>
- Gjerloev, J. W. (2012). The supermag data processing technique. *Journal of Geophysical Research*, *117*(A9), A09213. <https://doi.org/10.1029/2012JA017683>
- Grocott, A., Wild, J. A., Milan, S. E., & Yeoman, T. K. (2009). Superposed epoch analysis of the ionospheric convection evolution during substorms: Onset latitude dependence. *Annales Geophysicae*, *27*(2), 591–600. <https://doi.org/10.5194/angeo-27-591-2009>
- Haaland, S. E., Paschmann, G., Förster, M., Quinn, J. M., Torbert, R. B., McIlwain, C. E., et al. (2007). High-latitude plasma convection from cluster EDI measurements: Method and IMF-dependence. *Annales Geophysicae*, *25*, 239–253. <https://doi.org/10.5194/angeo-25-239-2007>
- Hesse, M. & Birn, J. (1990). Magnetic reconnection in the magnetotail current sheet for varying cross-tail magnetic field. *Geophysical Research Letters*, *17*(11), 2019–2022. <https://doi.org/10.1029/g1017i011p02019>
- Holappa, L., Asikainen, T., & Mursula, K. (2020). Explicit IMF B_y -dependence in geomagnetic activity: Modulation of precipitating electrons. *Geophysical Research Letters: Space Science*, *47*(4), e2019GL086676. <https://doi.org/10.1029/2019gl086676>
- Holappa, L., & Mursula, K. (2018). Explicit IMF B_y -dependence in high-latitude geomagnetic activity. *Journal of Geophysical Research: Space Science*, *123*, 4728–4740. <https://doi.org/10.1029/2018JA025517>
- Holappa, L., Mursula, K., Asikainen, T., & Richardson, I. G. (2014). Annual fractions of high-speed streams from principal component analysis of local geomagnetic activity. *Journal of Geophysical Research: Space Science*, *119*(6), 4544–4555. <https://doi.org/10.1002/2014JA019958>
- Holappa, L., Robinson, R. M., Pulkkinen, A., Asikainen, T., & Mursula, K. (2021). Explicit IMF B_y -dependence in geomagnetic activity: Quantifying ionospheric electrodynamics. *Journal of Geophysical Research: Space Science*, *126*, e2021JA029202. <https://doi.org/10.1029/2021ja029202>
- Hones, E. W. (1979). Plasma flow in the magnetotail and its implications for substorm theories. In S.-I. Akasofu (Ed.), *Dynamics of the magnetosphere* (Vol. 78, pp. 545–562). Springer. https://doi.org/10.1007/978-94-009-9519-2_29
- Kan, J. R., & Lee, L. C. (1979). Energy coupling function and solar wind-magnetosphere dynamo. *Geophysical Research Letters*, *6*(7), 577–580. <https://doi.org/10.1029/g1006i007p00577>
- King, J. H., & Papitashvili, N. E. (2005). Solar wind spatial scales in and comparisons of hourly wind and ACE plasma and magnetic field data. *Journal of Geophysical Research*, *110*(A2), A02104. <https://doi.org/10.1029/2004ja010649>
- Laitinen, T. V., Palmroth, M., Pulkkinen, T. I., Janhunen, P., & Koskinen, H. E. J. (2007). Continuous reconnection line and pressure-dependent energy conversion on the magnetopause in a global MHD model. *Journal of Geophysical Research*, *112*(A11). <https://doi.org/10.1029/2007ja012352>
- Liou, K. (2010). Polar Ultraviolet Imager observation of auroral breakup. *Journal of Geophysical Research*, *115*(12), 1–7. <https://doi.org/10.1029/2010JA015578>
- Liou, K., & Newell, P. T. (2010). On the azimuthal location of auroral breakup: Hemispheric asymmetry. *Geophysical Research Letters*, *37*(23), L23103. <https://doi.org/10.1029/2010GL045537>
- Liou, K., Newell, P. T., Sibeck, D. G., Meng, C.-I., Brittnacher, M., & Parks, G. (2001). Observation of IMF and seasonal effects in the location of auroral substorm onset. *Journal of Geophysical Research*, *106*(A4), 5799–5810. <https://doi.org/10.1029/2000JA003001>
- Liou, K., Sotirelis, T., & Mitchell, E. (2020). Control of the east-west component of the interplanetary magnetic field on the occurrence of magnetic substorms. *Geophysical Research Letters: Space Science*, *47*(5), e2020GL087406. <https://doi.org/10.1029/2020GL087406>
- Lockwood, M. (2019). Does adding solar wind poynting flux improve the optimum solar wind-magnetosphere coupling function? *Journal of Geophysical Research: Space Science*, *124*(7), 5498–5515. <https://doi.org/10.1029/2019ja026639>
- Lockwood, M., Bentley, S. N., Owens, M. J., Barnard, L. A., Scott, C. J., Watt, C. E., et al. (2019). The development of a space climatology: 1. Solar wind magnetosphere coupling as a function of timescale and the effect of data gaps. *Space Weather*, *17*(1), 133–156. <https://doi.org/10.1029/2018sw001856>
- McPherron, R. L., & Chu, X. (2017). The mid-latitude positive bay and the mpb index of substorm activity. *Space Science Reviews*, *206*(1–4), 91–122. <https://doi.org/10.1007/s11214-016-0316-6>
- McPherron, R. L., & Chu, X. (2018). The midlatitude positive bay index and the statistics of substorm occurrence. *Journal of Geophysical Research: Space Physics*, *123*(4), 2831–2850. <https://doi.org/10.1002/2017JA024766>
- Meurant, M., Gerard, J.-C., Blockx, C., Spanswick, E., Donovan, E. F., Hubert, B., et al. (2007). el - A possible indicator to monitor the magnetic field stretching at global scale during substorm expansive phase: Statistical study. *Journal of Geophysical Research*, *112*(A5). <https://doi.org/10.1029/2006ja012126>
- Milan, S. E., Gosling, J. S., & Hubert, B. (2012). Relationship between interplanetary parameters and the magnetopause reconnection rate quantified from observations of the expanding polar cap. *Journal of Geophysical Research*, *117*(A3). <https://doi.org/10.1029/2011ja017082>
- Milan, S. E., Grocott, A., & Hubert, B. (2010). A superposed epoch analysis of auroral evolution during substorms: Local time of onset region. *Journal of Geophysical Research*, *115*(May), 1–9. <https://doi.org/10.1029/2010JA015663>
- Milan, S. E., Provan, G., & Hubert, B. (2007). Magnetic flux transport in the Dungey cycle: A survey of dayside and nightside reconnection rates. *Journal of Geophysical Research*, *112*(1), A01209. <https://doi.org/10.1029/2006JA011642>
- Milan, S. E., Walach, M. T., Carter, J. A., Sangha, H., & Anderson, B. J. (2019). Substorm onset latitude and the steadiness of magnetospheric convection. *Journal of Geophysical Research: Space Physics*, *124*(3), 1738–1752. <https://doi.org/10.1029/2018JA025969>
- Myllys, M., Partamies, N., & Juusola, L. (2015). Latitude dependence of long-term geomagnetic activity and its solar wind drivers. *Annales Geophysicae*, *33*(5), 573–581. <https://doi.org/10.5194/angeo-33-573-2015>
- Newell, P. T., & Gjerloev, J. W. (2011). Evaluation of SuperMAG auroral electrojet indices as indicators of substorms and auroral power. *Journal of Geophysical Research*, *116*(A12). <https://doi.org/10.1029/2011ja016779>
- Newell, P. T., Sergeev, V. A., Bikkuzina, G. R., & Wing, S. (1998). Characterizing the state of the magnetosphere: Testing the ion precipitation maxima latitude (b2i) and the ion isotropy boundary. *Journal of Geophysical Research*, *103*(A3), 4739–4745. <https://doi.org/10.1029/97ja03622>

- Newell, P. T., Sotirelis, T., Liou, K., Meng, C.-I., & Rich, F. J. (2007). A nearly universal solar wind-magnetosphere coupling function inferred from 10 magnetospheric state variables. *Journal of Geophysical Research*, *112*(A1). <https://doi.org/10.1029/2006ja012015>
- Nosé, M., Iyemori, T., Wang, L., Hitchman, A., Matzka, J., Feller, M., & Celik, C. (2012). Wp index: A new substorm index derived from high-resolution geomagnetic field data at low latitude. *Space Weather*, *10*(8). <https://doi.org/10.1029/2012sw000785>
- Oberhagemann, L. R., & Mann, I. R. (2020). A new substorm onset mechanism: Increasingly parallel pressure anisotropic ballooning. *Geophysical Research Letters: Space Science*, *47*(2), e2019GL085271. <https://doi.org/10.1029/2019gl085271>
- Ohma, A., Østgaard, N., Reistad, J. P., Tenfjord, P., Laundal, K. M., Moretto Jørgensen, T., et al. (2019). Observations of asymmetric lobe convection for weak and strong tail activity. *Journal of Geophysical Research: Space Physics*, *124*. <https://doi.org/10.1029/2019ja026773>
- Ohma, A., Reistad, J. P., & Hatch, S. M. (2021). Modulation of magnetospheric substorm frequency: Dipole tilt and imf B_y effects. *Journal of Geophysical Research: Space Science*, e2020JA028856. <https://doi.org/10.1029/2011GL046767>
- Østgaard, N., Laundal, K. M., Juusola, L., Ásnes, A., Haaland, S. E., & Weygand, J. M. (2011). Interhemispherical asymmetry of substorm onset locations and the interplanetary magnetic field. *Geophysical Research Letters*, *38*(8), L08104. <https://doi.org/10.1029/2011GL046767>
- Petrukovich, A. A. (2011). Origins of plasma sheet B_y . *Journal of Geophysical Research*, *116*(A7). <https://doi.org/10.1029/2010ja016386>
- Reistad, J. P., Laundal, K. M., Ohma, A., Moretto, T., & Milan, S. E. (2020). An explicit IMF B_y dependence on solar wind-magnetosphere coupling. *Geophysical Research Letters*, *47*(1), e2019GL086062. <https://doi.org/10.1029/2019gl086062>
- Schindler, K., & Birn, J. (1993). On the cause of thin current sheets in the near-earth magnetotail and their possible significance for magnetospheric substorms. *Journal of Geophysical Research*, *98*(A9), 15477–15485. <https://doi.org/10.1029/93ja01047>
- Sergeev, V. A., & Gvozdevsky, B. B. (1995). MT-index- A possible new index to characterize the magnetic configuration of magnetotail. *Annales Geophysicae*, *13*(10), 1093–1103. <https://doi.org/10.1007/s00585-995-1093-9>
- Sergeev, V. A., Malkov, M., & Mursula, K. (1993). Testing the isotropic boundary algorithm method to evaluate the magnetic field configuration in the tail. *Journal of Geophysical Research*, *98*(A5), 7609–7620. <https://doi.org/10.1029/92ja02587>
- Shen, C., Li, X., Dunlop, M., Liu, Z., Balogh, A., Baker, D., et al. (2003). Analyses on the geometrical structure of magnetic field in the current sheet based on cluster measurements. *Journal of Geophysical Research*, *108*(A5). <https://doi.org/10.1029/2002ja009612>
- Smith, A. R. A., Beggan, C. D., Macmillan, S., & Whaler, K. A. (2017). Climatology of the auroral electrojets derived from the along-track gradient of magnetic field intensity measured by POGO, Magsat, CHAMP, and Swarm. *Space Weather*, *15*(10), 1257–1269. <https://doi.org/10.1002/2017SW001675>
- Snekvik, K., Tanskanen, E., Østgaard, N., Juusola, L., Laundal, K., Gordeev, E., et al. (2012). Changes in the magnetotail configuration before near-earth reconnection. *Journal of Geophysical Research*, *117*(A2). <https://doi.org/10.1029/2011ja017040>
- Tanskanen, E., Pulkkinen, T. I., Koskinen, H. E. J., & Slavin, J. A. (2002). Substorm energy budget during low and high solar activity: 1997 and 1999 compared. *Journal of Geophysical Research*, *107*, 1086. <https://doi.org/10.1029/2001JA900153>
- Tenfjord, P., Østgaard, N., Snekvik, K., Laundal, K. M., Reistad, J. P., Haaland, S., et al. (2015). How the IMF B_y induces a B_y component in the closed magnetosphere and how it leads to asymmetric currents and convection patterns in the two hemispheres. *Journal of Geophysical Research: Space Physics*, *120*(11), 9368–9384. <https://doi.org/10.1002/2015ja021579>
- Vasyliunas, V. M., Kan, J. R., Siscoe, G. L., & Akasofu, S.-I. (1982). Scaling relations governing magnetospheric energy transfer. *Planetary and Space Science*, *30*(4), 359–365. [https://doi.org/10.1016/0032-0633\(82\)90041-1](https://doi.org/10.1016/0032-0633(82)90041-1)